

PCCP

Accepted Manuscript



This is an *Accepted Manuscript*, which has been through the Royal Society of Chemistry peer review process and has been accepted for publication.

Accepted Manuscripts are published online shortly after acceptance, before technical editing, formatting and proof reading. Using this free service, authors can make their results available to the community, in citable form, before we publish the edited article. We will replace this *Accepted Manuscript* with the edited and formatted *Advance Article* as soon as it is available.

You can find more information about *Accepted Manuscripts* in the [Information for Authors](#).

Please note that technical editing may introduce minor changes to the text and/or graphics, which may alter content. The journal's standard [Terms & Conditions](#) and the [Ethical guidelines](#) still apply. In no event shall the Royal Society of Chemistry be held responsible for any errors or omissions in this *Accepted Manuscript* or any consequences arising from the use of any information it contains.

Optical absorption of warped nanographenes tuned by five- and seven-membered carbon rings[†]

Xinqin Wang,^a Shengping Yu,^b Zhaoyang Lou,^a Qun Zeng,^a and Mingli Yang^{*a}

^a Institute of Atomic and Molecular Physics, Key Laboratory of High Energy Density Physics and Technology of Ministry of Education, Sichuan University, Chengdu 610065, P. R. China

^b College of Chemistry and Environment Protection Engineering, Southwest University for Nationalities, Chengdu 610041, P. R. China

[†] Electronic supplementary information (ESI) available. See DOI

Abstract

The introduction of multiple carbon rings is one of the common ways for graphene modification. Starting from warped $C_{80}H_{30}$ nanographene, which consists of a number of six- and seven-membered carbon rings (C6 and C7) centering at a five-membered carbon ring (C5), we explored the structure and property variations of its derivatives in which their C7 rings were gradually replaced with C6 rings. With reducing number of C7 rings, their curved boundary with the C6 rings becomes flat until a bowl-like structure is formed when all the C7 rings disappear. The optical absorption spectra vary accordingly. Both the α -bands and the maximum absorption bands in the visible region are related to the number and location of the C7 rings. Further analysis on the excited states of the $C_{80}H_{30}$ derivatives, as well as on the designed model systems revealed that the C7 rings affect the electron excitations in two ways. In addition to their participation in electronic transitions, they control the composition of molecular orbitals that are involved in the excitations. The highest occupied molecular orbitals are mainly contributed by atoms on the C6 and C7 rings, while the lowest unoccupied molecular orbitals by atoms on the C5 and C6 rings. Our study sheds some light on how the multiple carbon rings affect the optical absorption of nanographenes and provides information for the preparation of nanographenes with tunable structural and optical properties.

1. INTRODUCTION

Nano-carbon materials are nowadays of particular interest both in research and applications. Zero-dimensional fullerenes, one-dimensional carbon nanotubes, and two-dimensional graphenes make up the family of nanocarbons. Graphenes and their derivatives are known for their superior mechanical, thermal, electronic, optical, and chemical properties.¹⁻⁹ It is believed that graphene-based materials will affect our life deeply in the future. Tremendous effort has been devoted to discover new features and applications of graphenes by means of physical induction and/or chemical modification. For instance, Krepel *et al.*¹⁰ introduced phenyl and lithium atom onto graphene and characterized the interaction among them. Archambault and Rochefort¹¹ found that Au, Pd, and Ti atoms adsorb onto graphene and alter its band gap regularly, suggesting chemical adsorption as an effective way to adjust its electronic properties.

In addition to chemical adsorption on the graphene surface, modifications to the graphene itself have also been explored. The strategy of introducing functional groups or cyclic hydrocarbons to control the structure and property variations of graphenes has been addressed by many authors.¹²⁻³⁴ Crespi *et al.*²¹ reported a metallic sheet with high density of states around the Fermi level by creating defects in the honeycomb lattice. Terrones *et al.*²² found the rolled and seamless graphene has a well-defined metallic behavior. Hudspeth *et al.*²³ studied the electronic properties and relative stability of the biphenylene sheet composed of alternating eight-, six-, and four-carbon rings, as well as its ribbon and tube derivatives of different widths and chiralities, showing that the two-dimensional sheet presents a metallic character. Graphene with extended line defects that consist of five- and eight-carbon rings has

been synthesized by Lahiri *et al.*²⁴ and its magnetic properties and half metallic characters have been studied theoretically and experimentally.²⁵⁻²⁷ Using a generalized von Karman equation Zhang *et al.*²⁸ investigated the graphene wrinkling induced by a prescribed distribution of topological defects such as disclinations (heptagons or pentagons) and dislocations (heptagon–pentagon dipoles). Yang *et al.*²⁹ reported a new class of conjugated polycyclic molecules for applications in organic electronic devices. These molecules have a nearly flat polycyclic framework with a *p*-quinodimethane core. Evans *et al.*³⁰ synthesized a carbon nanohoop that can be envisaged as an open tubular fragment of C₆₀, the equator of C₇₀ fullerene and the unit cycle of a [5, 5] armchair carbon nanotube. A facile and efficient self-sorting assemble (CSA) strategy has been reported by Zhang *et al.*³¹ for a bottom-up construction of the 3-fold symmetrical and highly substituted hexa-cata-hexabenzocoronenes (*c*-HBCs), which have large disc-shaped PAHs and can be served as new launching platforms for the construction of larger and more complex π -conjugated molecules and supramolecular architectures. Shimizu *et al.*³² have revealed that the introduction of a seven-membered-ring unit in the place of a five-membered-ring unit in the structure of subphthalocyanine resulted in significant distortion of the bowl-shaped structure of the conjugated molecule as well as unprecedented property changes.

Recently, a new kind of grossly warped graphene was reported by Kawasumi *et al.*,³³ which has unique structural and physical properties, such as facile bowl-to-bowl inversion of the central corannulene, a widened highest occupied molecular orbital (HOMO)–lowest unoccupied molecular orbital (LUMO) gap, etc. Dai *et al.*³⁴ performed density functional theory (DFT) calculations on the warped graphenes, predicting them as a promising nonlinear

optical material.

These studies have manifested the important role of multiple carbon rings (MCR) in the chemical modification of graphene structures and properties. Although the consequences of introducing MCR into graphenes have been addressed by several authors,^{23, 32} a systematic study of the MCR effect on the structural and properties is still lack. Starting from the warped nanographene, we investigated in this work how the arrangement of five- and seven-membered carbon rings in a graphene alters its structure and optical properties by means of DFT calculations. These two kinds of odd-numbered rings have different effects on the graphene structures. Five-membered rings (referred to as C5 hereafter) impart geodesic curvature, while seven-membered rings (referred to as C7 hereafter) introduce so-called 'negative curvature'.³³ In a microscopic view, C5 and C7 exhibit different aromaticity from a six-membered carbon ring (referred to as C6 hereafter). The introduction of C5 and C7 should affect significantly the electronic structure of C6-made graphene. In order to investigate the MCR effect on the structure and optical properties of graphene, a number of warped nanographenes with different numbers and locations of five- and seven-membered rings were designed, and their optical absorption spectra were predicted with time-dependent DFT calculations (TDDFT). The variations in the optical absorption bands were further rationalized with a model study on a series systems comprising of five-, six- and seven-membered rings. The purpose of this study is to provide information for the design strategy of warped nanographenes with expected structural and optical properties.

2. COMPUTATIONAL METHOD

The initial structures of warped $C_{80}H_{30}$ and planar $C_{78}H_{30}$ were taken from experiments.^{33, 35} Starting from the $C_{80}H_{30}$ structure a series of derivatives with various numbers of C7 rings were designed by modifying the backbones together with reducing carbon atoms or adding hydrogen atoms. The C5 ring and its surrounding C6 rings keep unchanged in these designed complexes, while the number of C7 rings varies from 1 to 7, and the number of C6 rings changes accordingly. All these structures were optimized with the Perdew-Burke-Ernzerhof (PBE)^{36, 37} and B3LYP³⁸⁻⁴⁰ exchange–correlation functionals, as implemented in Turbomole suite⁴¹. The triple-zeta basis set def-TZVP^{42, 43} was used. The density convergence tolerance was set to 10^{-6} a.u in the self-consistent field calculations, and the convergence criteria were set to 10^{-4} a.u. for the gradient and 10^{-6} a.u. for energy in geometry optimization. The resolution-of-the-identity (RI) approximation^{44, 45} and multiple accelerated RI (MARI) approach⁴⁶ were applied to speed up the calculations.

TDDFT⁴⁷⁻⁴⁹ calculations were performed to predict the optical absorption spectra of warped $C_{80}H_{30}$ and planar $C_{78}H_{30}$ with various functionals, such as B3LYP, CAM-B3LYP⁵⁰, PBE, PBE0⁵¹, TPSSH⁵² and M06-2X⁵³, since the predicted spectra were found functional-dependent. By comparing with the measured spectra, B3LYP was selected for the computations of designed complexes. The TDDFT calculations were carried out with Gaussian09 software⁵⁴ using the 6-31G(d, p) basis set, and the SCF convergence criteria were tightened to 10^{-8} a.u in density. The lowest 50 excitations were calculated, which are large enough to produce the absorption bands of interest. The polarizable continuum model (PCM)⁵⁵ with dielectric constants of 8.93 and 2.61 were employed to simulate the experimental environment of dichloromethane and carbon disulfide, respectively.

3. RESULTS AND DISCUSSION

3.1 Structure and optical absorption of $C_{80}H_{30}$ and $C_{78}H_{30}$.

The optimized $C_{80}H_{30}$ structure is shown in Fig. 1. It centers at a C5 ring that is surrounded by five C6 rings, and then by five C7 rings. Five C6 rings are also formed among the C7 rings and the inner C6 rings. At the outermost of $C_{80}H_{30}$ are ten C6 rings that are adjacent to the C7 rings. The $C_{80}H_{30}$ looks like a saddle with two double concave surfaces. The bending occurs at the C6 and C7 ring junctions. Table 1 presents the averaged C–C bondlengths in different rings. The computed bondlengths are in well agreement with the measurement³³. For the C5 ring, its averaged C–C distance is 1.405 Å, while the C6 rings have averaged C–C distances of 1.399–1.426 Å. The five C7 rings have similar C–C distances about 1.45 Å. Since most of the C–C bonds are shared by two adjacent rings, one can distinguish the bonds with these two rings. As in fullerenes, r_{56} denotes the length of C–C bond shared by C5 and C6 rings, and r_{66} for bonds shared by two C6 rings. The computed averaged r_{56} , r_{66} and r_{67} are 1.405, 1.406, and 1.448 Å, respectively, which are quite different from the C–C distances in C_{60} (1.45 ± 0.015 Å for r_{56} and 1.40 ± 0.015 Å for r_{66} ²⁰). The bending in $C_{80}H_{30}$ is measured with the dihedral angles, as shown in Fig. S1 in the ESI. Some of the dihedral angles reach about 145° at the C6 and C7 junctions, while the bending is less significant between C5 and C6 rings. Fig. 1 also shows the optimized structure of $C_{78}H_{30}$, which is planar with D_{6h} symmetry. The average C–C bondlength is 1.416Å, which is almost as long as those in graphene (1.420 Å^{18}), but longer than those in benzene (1.396 Å^{19}). From its center to the edge, the C–C bond changes from 1.418 Å to 1.399 Å, resulting from the edge effect of H passivation.

The predicted HOMO-LUMO gaps are 3.01 eV for $C_{80}H_{30}$ and 2.91 eV for $C_{78}H_{30}$, which are close with the B3LYP/6-31G(d, p) calculations (3.06 eV and 2.90 eV) by Kawasumi et al.³³ Although their gaps are similar, but the HOMO and LUMO orbitals of $C_{80}H_{30}$ and $C_{78}H_{30}$ are quite different, as shown in Fig. 1. The HOMO of $C_{80}H_{30}$ distributes mainly on the C atoms shared by C6 and C7 rings, and the LUMO is on C atoms shared by C5 and C6 rings. In contrast to the localized distribution in $C_{80}H_{30}$, the HOMO and LUMO in $C_{78}H_{30}$ delocalize across all the C atoms. Their projected density of states (PDOS) was displayed in Fig. S2. For both structures, their DOS are contributed by the $2p$ components, indicating that the curving in $C_{80}H_{30}$ does not change the delocalized nature of the $2p$ electrons of C atoms. It is apparent that the delocalization in the HOMO and LUMO orbitals of $C_{78}H_{30}$ is more significant than that of $C_{80}H_{30}$.

The optical absorption of $C_{80}H_{30}$ was simulated using TDDFT calculations with various functionals. These functionals predict somewhat different spectra, as shown in Fig. S3. The predicted first peaks cover a wide range, about 583 nm for PBE, but about 403 nm for CAM-B3LYP and M06-2X. We noticed that B3LYP and PBE0 produce similar results both in band location and shape. Compared to the measurement (491 nm),³³ moreover, B3LYP gives better result (486 nm) than other functionals. The second (444 nm) and the strongest (435 nm) bands also match well with the measurement (452 nm and 418 nm),³³ respectively. The GW (Green's function G and screened Coulomb interaction W) + BSE (Bethe-Salpeter equation) approach was used by Noguchi and Sugino⁵⁶ to compute the absorption spectra of $C_{80}H_{30}$, giving the first three bands at 460, 422 and 393 nm, respectively. Therefore, B3LYP was selected to compute the optical absorption of $C_{80}H_{30}$ derivative in the subsequent TDDFT

calculations. The B3LYP predicted spectra of $C_{80}H_{30}$ and $C_{78}H_{30}$ were compared in Fig. 1. $C_{78}H_{30}$ has its maximum absorption at about 447 nm, which is also the first peak. In the measurement³⁵, the absorption peaks at 440 nm and has a very wide shoulder reaching about 525 nm.

3.2 Structure and optical absorption of $C_{80}H_{30}$ derivatives.

The $C_{80}H_{30}$ structures were modified by changing the number and location of $C7$ rings. Two approaches were used to reduce the $C7$ number. In the first approach, one C atom in the $C7$ ring and one C atom in its adjacent ring were removed and the $C7$ ring was transformed into a $C6$ ring. Two linked H atoms were also removed to keep the conjugated framework. Seven structures with different $C7$ numbers and locations were built in this way. The optimized structures are shown in Fig. 2, labeled as **a** ($C_{78}H_{28}$), **b1** and **b2** (two isomers of $C_{76}H_{26}$), **c1** and **c2** (two isomers of $C_{74}H_{24}$), **d** ($C_{72}H_{22}$), and **e** ($C_{70}H_{20}$). From **a** to **e**, the number of $C7$ ring decreases from four to zero. **b1** and **b2** have three $C7$ rings, and **c1** and **c2** have two $C7$ rings, but the ring locations are different. The molecular structures change remarkably when a $C7$ changes into a $C6$. The bending site in the $C7$ disappears and the atoms nearby tends to become planar. With decreasing $C7$ ring, the curved $C_{80}H_{30}$ changes into a bowl-shaped $C_{70}H_{20}$ with an arm-chair edge.

Fig. 2 shows the B3LYP/6-31G(d, p) computed optical absorption spectra of **a–e**. Some similarity and differences were noted in the spectra. First, the band distributions of **a–d** are similar with that of $C_{80}H_{30}$, and with each other. They all have a small α band that is followed by a big β band. The other bands are also similar to some extent in shape. Compared to $C_{80}H_{30}$,

next, the first peaks of **a–d** redshift by about 29–46 nm, while the red shifts of the β bands are about 21–31 nm. The first peaks vary from 514 nm to 531 nm when the C7 number changes from four to one. The β bands in most complexes are the maximum absorption in the visible region, ranging from 454 nm to 464 nm. Third, the location of C7 has some influence on the spectra. Although the band locations are basically similar for **b1** and **b2**, their relative band strengths changes. The β band is no longer the maximum in the spectra of **b2**. The band shapes are similar for **c1** and **c2**, but a shift of about 15 nm occurs for their β bands. Finally, the spectra of **e** are quite different from those of other derivatives. Its first peak, the maximum absorption, is at 454 nm, and its β band moves to 339 nm. Therefore, the disappearance of C7 leads to dramatic change in the absorption spectra of $C_{80}H_{30}$ derivatives.

Alternatively, $C_{80}H_{30}$ was modified by breaking one C–C bond in C7 and adding two H atoms. In this way the number of C atoms keeps unchanged while the number of C7 is reduced. Six structures, $C_{80}H_{32}$ (**a'**), $C_{80}H_{34}$ (two isomer **b1'** and **b2'**), $C_{80}H_{36}$ (**c'**), $C_{80}H_{38}$ (**d'**) and $C_{80}H_{40}$ (**e'**), were constructed and optimized, as show in Fig. 3. Similar to **a–e**, the bending sites in the C7 moiety becomes planar and the curved $C_{80}H_{30}$ structure changes into a bowl-shaped $C_{80}H_{40}$ ultimately. Unlike the arm-chair edge of **e**, **e'** has its edge made of protruding phenyl rings.

Derivatives **a'–e'** have the same number of carbon atoms, and similar conjugation path. Fig. 3 shows their predicted absorption spectra. Again, some similarity and differences were noted in these spectra. First, compared to the spectra of $C_{80}H_{30}$, the first and small peaks remain for **a'–d'** whose locations are about 479–505 nm. However, the big β band in $C_{80}H_{30}$ is split into two bands, both are stronger than the α -band. Next, the band distributions of **a'–d'** are similar.

They all have a small α band and big β and γ bands. The β and γ bands are at 412–454 nm and 344–422 nm, respectively. Third, the different C7 locations in **b1'** and **b2'** have little effect on the band shapes, but lead to a small shift in the β and γ bands. Finally, both the band shape and location vary when the last C7 disappears. A big α band at 426 nm, which shifts toward the short-wavelength direction by 59 nm, was predicted for **e'**.

The spectra of **a–e** and **a'–e'** are different in several aspects. The maximum absorption in the visible region of **a–d** is the β band, which is split into two bands, and no longer the maximum for **a'–d'**, resulting in a rather different band distribution for these two families of designed derivatives. Moreover, a blue shift was noted for **a'–e'** with respect to the corresponding bands of **a–e**. For example, the α - and β -bands of **a** peak at 514 nm and 458 nm, while the corresponding bands of **a'** are at 492 nm and 432 nm, respectively, resulting from the relatively small conjugation systems of **a–e**. The spectra of **e** in the studied region are composed of a big α -band and several much smaller bands, while the α -band of **e'** slightly smaller than the β - and γ -bands. The peaks of their α -bands are also different, 454 nm for **e** and 426 nm for **e'**.

Therefore, the optical absorption of warped nanographenes can be tuned by controlling their numbers and locations of C7 rings. For $C_{80}H_{30}$, its first absorption peak varies from 460 nm to 525 nm when the C7 rings are gradually replaced with C6 rings, while the maximum absorption in the visible region from 430 nm to 465 nm. Such adjustment in the absorption bands is inevitably decided by the variations in their electronic structures. Table S2 presents the main compositions of the α -bands and the maximum absorption bands in the visible region of $C_{80}H_{30}$, $C_{78}H_{30}$, **a–e** and **a'–e'**. For most complexes their first excitations are

associated with the HOMO-LUMO transitions, while their maximum absorptions with several more lower occupied orbitals and/or higher unoccupied orbitals. Fig. S4 and Fig. S5 shows the HOMO and LUMO contours of **a-e** and **a'-e'**, in comparison with those of $C_{80}H_{30}$ and $C_{78}H_{30}$ in Fig. 1. The HOMOs of the warped complexes are mainly contributed by atoms in the C6 and C7 rings, while the LUMOs by atoms in the C5 and C6 rings. In addition, only small part of atoms is involved in the HOMO and LUMO of $C_{80}H_{30}$. With the decreasing C7 number, more and more atoms contribute to the HOMO and LUMO. One can find that the HOMO and LUMO of **e** in Fig. S4 are similar to those of $C_{78}H_{30}$. It is evident that the C7 rings in the warped nanographenes affect the optical absorption in two ways. The first is that the C7 rings themselves contribute to the constitution of the HOMO orbitals, and the second is that the C7 rings reduce the delocalization zone of electrons.

3.3 Model systems with C5, C6 and C7 rings.

In order to understand the structural and optical property variations in the $C_{80}H_{30}$ derivatives, we designed four families of model systems and compared their electronic structures. Fig. 4 displays the structures of the four model systems. A CH_2 group was added to the C5 and C7 rings to keep their conjugation like in the nanographene. These structures were optimized with B3LYP/def-TZVP. The HOMO-LUMO gaps of these model molecules are presented in Table 2 and their HOMO and LUMO contours in Fig. S6.

In Model I, the molecules center at a phenyl ring which connects with two C5, C6 or C7 rings at its two sides. All the optimized structures are planar. The molecule of C6-C6-C6 rings has a narrower gap than benzene, resulting from its larger conjugation zone. But its gap is

wider than that of C5-C6-C5 by 1.59 eV, implying that the replacement of C6 with C5 favors the HOMO-LUMO electron transition. The replacement of C6 with C7, or C5 with C7, further lowers the gap in C7-C6-C7 and C5-C6-C7, indicating that the introduction of C7 ring also favors the HOMO-LUMO transition. Since the electron-rich C7 ring has greater tendency to lose its electron than the electron-deficient C5 ring, the molecules with C7 ring(s) have lower gaps than C5-C6-C5. Further analysis shows that C7 ring raises the HOMO, while C5 and C7 lower the LUMO. The HOMO and LUMO contours shows that the electron transition occurs from the C7 ring to the C5 and C6 rings, similar to the transitions of the C₈₀H₃₀ derivatives. However, things are different when C5 and C7 appear in a molecule simultaneously, as we discussed below for Model II and III.

In Model II, a C5-C7 connection was set as a reference. One to three C6 rings were inserted between the C5 and C7 rings in the other model molecules. With increasing C6 on the chain, the HOMO-LUMO gap becomes wide, although the conjugation path elongates. Their HOMO covers all atoms in C6 and C7 rings, while their LUMO covers atoms in C5 and C6 rings. Therefore, electron excitation also occurs from C7 to C5 and C6 in their HOMO-LUMO transitions.

In Model III, all atoms in the model constitute a polycyclic aromatic hydrocarbon, and all the molecules have a C5 end. The molecular C5C6 has a wide gap of 4.15 eV that is narrowed to 3.84 eV when one more C6 is attached. When this C6 is replaced with C7, however, the gap lowers to 3.00 eV. When one more C6 is inserted, the gap widens to 3.32 eV. The HOMO and LUMO of C5C6 and C5C6C6 cover all carbon atoms. However, the HOMO of C5C6C7 and C5C6C6C7 cover atoms in C6 and C7, while their LUMO cover atoms in C5 and C6.

In Model IV, C5, C6 and C7 constitute a polycyclic aromatic hydrocarbon in which the C5 and C6 rings are kept in one plane, while the dihedral angle (φ) between C6 and C7 changes from 180° to 160° at an interval of 5° . The molecular geometries were fully optimized except constraints to the dihedral angles between C5 and C6 and between C6 and C7. When φ changes from 180° to 160° , the C7 ring deviates gradually from the C5 and C6 plane. Meanwhile, the C–C bonds near to the C6–C7 border are subjected to some changes up to 0.009\AA in bond-length and up to 3.1° in bond-angle. However, the variations in HOMO–LUMO gap are less than 0.022 eV , corresponding to a difference in wavelength of about 3 nm . Therefore, it is the number of C7 rings rather than the distortion caused by the C7 rings that has great influence on the optical absorption of nanographenes.

Computations on the model systems reveal several aspects. First, the introduction of C5, especially C7, tends to narrow the HOMO–LUMO gap, making its first excitation redshift. This is in accordance with our calculations for the $\text{C}_{80}\text{H}_{30}$ and its derivatives whose α -bands evidently redshifts compared to that of planar $\text{C}_{78}\text{H}_{30}$. Next, in absence of C7, all carbon atoms of molecules with C5 and C6 contribute to their HOMO and LUMO, which is similar to the situation of $\text{C}_{78}\text{H}_{30}$. This complies with the fact that $\text{C}_{78}\text{H}_{30}$ has similar α -band with the derivatives **e** and **e'** that are made up with only C5 and C6 rings. When both C5 and C7 are present, thirdly, C7 mainly contributes to the HOMO, while the role of C5 in excitation changes. The contribution of C5 decreases in HOMO, but increases in LUMO. The interplay of C5 and C7 makes the first excitation redshift further. Finally, our model study predicted that the C6 standing between C5 and C7 tends to blueshift the first excitation, resulting from its resistance to the electron flow between its two sides. A longer distance between C5 and C7

should lead to a shorter-wavelength excitation. The $C_{80}H_{30}$ derivatives designed have a fixed C5–C7 distance, and the effect of C6 bridge length was not studied in this work.

4. CONCLUSION

DFT and TDDF calculations were performed to study the effect of C5 and C6 rings on the structural and optical properties of nanographenes. Two families of nanographenes based on the experimentally prepared warped $C_{80}H_{30}$ were constructed. All these nanographenes center at a C5 ring, and have a number of C6 and C7 rings surrounded. The number and location of C6 and C7 were carefully designed. The structures were optimized using PBE and B3LYP functionals with def-TZVP basis set, and their optical absorption spectra were predicted with carefully selected functional, B3LYP, which produced results matching well with the observations for $C_{80}H_{30}$. With decreasing C7 number and increasing C6 number, the curved structure at their boundary gradually becomes planar. A bowl-like structure was formed when all C7 rings were replaced with C6 rings. The C–C bond-lengths are different in C5, C6 and C7 rings, and vary from molecular center to edge.

The optical absorption spectra vary with the C6/C7 replacement. Although the two families exhibit some different behaviors in their band distributions, they share some common features. The bowl-like structures with centered C5 show similar absorption bands with planar nanographene that consists of C6 rings. When C7 was introduced, however, different absorption spectra were obtained for the warped structures. A remarkable redshift in α -band was noted and the band distribution varies. Moreover, the α -bands and the maximum absorption bands in the visible region are related to the number and location of the C7 rings.

For $C_{80}H_{30}$, its first absorption peak varies from 460 nm to 525 nm when the C7 rings are gradually replaced with C6 rings, while the maximum absorption in the visible region from 430 nm to 465 nm. Therefore, the optical absorption of warped nanographenes can be tuned by controlling their numbers and locations of C7 rings among the C6 rings.

All these findings were further analyzed with four model systems. The introduction of C5, especially C7, tends to narrow the HOMO-LUMO gap. For molecules without C7, all carbon atoms in C5 contribute to both HOMO and LUMO, but its role in excitation changes when C7 is introduced. While C7 mainly contributes to the HOMO, the contribution of C5 decreases in HOMO, but increases in LUMO. Therefore, the C7 rings affect the optical absorption spectra of warped nanographenes by participating in electronic transitions and/or by changing the composition of molecular orbitals that are involved in the excitations.

ACKNOWLEDGEMENT

The authors thank financial support from National Natural Science Foundation of China (No. 21373140) and National High Technology Research and Development Program of China (No. 2015AA034202). Part of calculations was carried out at the State Key Laboratory of Physical Chemistry of Solid Surfaces, Xiamen University.

REFERENCES

- 1 D. C. Elias, R. R. Nair, T. M. G. Mohiuddin, S. V. Morozov, P. Blake, M. P. Halsall, A. C. Ferrari, D. W. Boukhvalov, M. I. Katsnelson, A. K. Geim and K. S. Novoselov, *Science*, 2009, **323**, 610-613.
- 2 F. Withers, M. Dubois and A. K. Savchenko, *Phys. Rev. B*, 2010, **82**, 073403.
- 3 M. Scardamaglia, S. Lisi, S. Lizzit, A. Baraldi, R. Larciprete, C. Mariani and M. G. Betti, *J. Phys. Chem. C*, 2013, **117**, 3019-3027.
- 4 L. A. Chernozatonskii, D. G. Kvashnin, P. B. Sorokin, A. G. Kvashnin and J. W. Bruning, *J. Phys. Chem. C*, 2012, **116**, 20035-20039.
- 5 J. T. Robinson, J. S. Burgess, C. E. Junkermeier, S. C. Badescu, T. L. Reinecke, F. K. Perkins, M. K. Zalalutdniov, J. W. Baldwin, J. C. Culbertson, P. E. Sheehan and E. S. Snow, *Nano Lett.*, 2010, **10**, 3001-3005.

- 6 J. Zhou, L. Wang, R. Qin, J. X. Zheng, W. N. Mei, P. A. Dowben, S. Nagase, Z. X. Gao and J. Lu, *J. Phys. Chem. C*, 2011, **115**, 25273-25280.
- 7 B. Li, L. Zhou, D. Wu, H. L. Peng, K. Yan, Y. Zhou and Z. F. Liu, *ACS Nano*, 2011, **5**, 5957-5961.
- 8 A. M. Silva, M. S. Pires, V. N. Freire, E. L. Albuquerque, D. L. Azevedo and E. W. S. Caetano, *J. Phys. Chem. C*, 2010, **114**, 17472-17485.
- 9 J. Takashiro, Y. Kudo, S. Kaneko, K. Takai, T. Ishii, T. Kyotani, T. Enoki and M. Kiguchi, *Phys. Chem. Chem. Phys.*, 2014, **16**, 7280-7289.
- 10 D. Krepel and O. Hod, *Surf. Sci.*, 2011, **605**, 1633-1642.
- 11 C. Archambault and A. Rochefort, *ACS Nano*, 2013, **7**, 5414-5420.
- 12 P. Rivero, C. A. Jimenez-Hoyos and G. E. Scuseria, *J. Phys. Chem. B*, 2013, **117**, 12750-12758.
- 13 Y. H. Lu, W. Chen, Y. P. Feng and P. M. He, *J. Phys. Chem. B*, 2009, **113**, 2-5.
- 14 W. Chen, S. Chen, D. C. Qi, X. Y. Gao and A. T. S. Wee, *J. Am. Chem. Soc.*, 2007, **129**, 10418-10422.
- 15 H. S. Kang, *J. Am. Chem. Soc.*, 2005, **127**, 9839-9843.
- 16 M. Baldoni and F. Mercuri, *Phys. Chem. Chem. Phys.*, 2015, **17**, 2088-2093.
- 17 A. M. Garay-Tapia, A. H. Romero and V. Barone, *J. Chem. Theory Comput.*, 2012, **8**, 1064-1071.
- 18 D. R. Cooper, B. D'Anjou, N. Ghattamaneni, B. Harack, M. Hilke, A. Horth, N. Majlis, M. Massicotte, L. Vandsburger, E. Whiteway and V. Yu, *Condens. Matter Phys.*, 2012, **2012**, 1-56.
- 19 J. Aihara, *Bull. Chem. Soc. Jpn.*, 1990, **63**, 1956-1960.
- 20 C. S. Yannoni, P. P. Bernier, D. S. Bethune, G. Meijer and J. R. Salem, *J. Am. Chem. Soc.*, 1991, **113**, 3190-3192.
- 21 V. H. Crespi, N. G. Chopra, M. L. Cohen, A. Zettl and S. G. Louie, *Phys. Rev. B*, 1996, **54**, 5927-5931.
- 22 H. Terrones, M. Terrones, E. Hernandez, N. Grobert, J. C. Charlier and P. M. Ajayan, *Phys. Rev. Lett.*, 2000, **84**, 1716-1719.
- 23 M. A. Hudspeth, B. W. Whitman, V. Barone and J. E. Peralta, *ACS Nano*, 2010, **4**, 4565-4570.
- 24 J. Lahiri, Y. Lin, P. Bozkurt, I. I. Oleynik and M. Batzill, *Nat. Nanotechnol.*, 2010, **5**, 326-329.
- 25 L. Z. Kou, C. Tang, W. L. Guo and C. F. Chen, *ACS Nano*, 2011, **5**, 1012-1017.
- 26 X. Q. Lin and J. Ni, *Phys. Rev. B*, 2011, **84**.
- 27 J. C. Ren, Z. J. Ding, R. Q. Zhang and M. A. Van Hove, *Phys. Rev. B*, 2015, **91**.
- 28 T. Zhang, X. Y. Li and H. J. Gao, *J. Mech. Phys. Solids*, 2014, **67**, 2-13.
- 29 X. J. Yang, D. Q. Liu and Q. Miao, *Angew. Chem. Int. Ed.*, 2014, **53**, 6786-6790.
- 30 P. J. Evans, E. R. Darzi and R. Jasti, *Nat. Chem.*, 2014, **6**, 404-408.
- 31 Q. Zhang, H. Q. Peng, G. S. Zhang, Q. Q. Lu, J. Chang, Y. Y. Dong, X. Y. Shi and J. F. Wei, *J. Am. Chem. Soc.*, 2014, **136**, 5057-5064.
- 32 S. Shimizu, S. Nakano, A. Kojima and N. Kobayashi, *Angew. Chem. Int. Ed.*, 2014, **53**, 2408-2412.
- 33 K. Kawasumi, Q. Y. Zhang, Y. Segawa, L. T. Scott and K. Itami, *Nat. Chem.*, 2013, **5**, 739-744.
- 34 Y. F. Dai, Z. Y. Li and J. L. Yang, *J. Phys. Chem. C*, 2014, **118**, 3313-3318.

- 35 F. Dotz, J. D. Brand, S. Ito, L. Gherghel and K. Mullen, *J. Am. Chem. Soc.*, 2000, **122**, 7707-7717.
- 36 J. P. Perdew, K. Burke and M. Ernzerhof, *Phys. Rev. Lett.*, 1996, **77**, 3865-3868.
- 37 J. P. Perdew and Y. Wang, *Phys. Rev. B*, 1992, **45**, 13244-13249.
- 38 A. D. Becke, *Phys. Rev. A*, 1988, **38**, 3098-3100.
- 39 C. T. Lee, W. T. Yang and R. G. Parr, *Phys. Rev. B*, 1988, **37**, 785-789.
- 40 A. D. Becke, *J. Chem. Phys.*, 1993, **98**, 5648-5652.
- 41 TURBOMOLE, v5-9-1, University of Karlsruhe, 2007.
- 42 K. Eichkorn, F. Weigend, O. Treutler and R. Ahlrichs, *Theor. Chem. Acc.*, 1997, **97**, 119-124.
- 43 A. Schafer, C. Huber and R. Ahlrichs, *J. Chem. Phys.*, 1994, **100**, 5829-5835.
- 44 K. Eichkorn, O. Treutler, H. Ohm, M. Haser and R. Ahlrichs, *Chem. Phys. Lett.*, 1995, **242**, 652-660.
- 45 F. Weigend and M. Haser, *Theor. Chem. Acc.*, 1997, **97**, 331-340.
- 46 M. Sierka, A. Hogeckamp and R. Ahlrichs, *J. Chem. Phys.*, 2003, **118**, 9136-9148.
- 47 R. Bauernschmitt and R. Ahlrichs, *Chem. Phys. Lett.*, 1996, **256**, 454-464.
- 48 M. E. Casida, C. Jamorski, K. C. Casida and D. R. Salahub, *J. Chem. Phys.*, 1998, **108**, 4439-4449.
- 49 C. Van Caillie and R. D. Amos, *Chem. Phys. Lett.*, 1999, **308**, 249-255.
- 50 T. Yanai, D. P. Tew and N. C. Handy, *Chem. Phys. Lett.*, 2004, **393**, 51-57.
- 51 C. Adamo and V. Barone, *J. Chem. Phys.*, 1999, **110**, 6158-6170.
- 52 J. M. Tao, J. P. Perdew, V. N. Staroverov and G. E. Scuseria, *Phys. Rev. Lett.*, 2003, **91**, 146401-146404.
- 53 Y. Zhao and D. G. Truhlar, *Theor. Chem. Acc.*, 2008, **120**, 215-241.
- 54 M. J. Frisch, G. W. Trucks, H. B. Schlegel, G. E. Scuseria, M. A. Robb, J. R. Cheeseman, G. Scalmani, V. Barone, B. Mennucci, G. A. Petersson, H. Nakatsuji, M. Caricato, X. Li, H. P. Hratchian, A. F. Izmaylov, J. Bloino, G. Zheng, J. L. Sonnenberg, M. Hada, M. Ehara, K. Toyota, R. Fukuda, J. Hasegawa, M. Ishida, T. Nakajima, Y. Honda, O. Kitao, H. Nakai, T. Vreven, J. J. A. Montgomery, J. E. Peralta, F. Ogliaro, M. Bearpark, J. J. Heyd, E. Brothers, K. N. Kudin, V. N. Staroverov, R. Kobayashi, J. Normand, K. Raghavachari, A. Rendell, J. C. Burant, S. S. Iyengar, J. Tomasi, M. Cossi, N. Rega, J. M. Millam, M. Klene, J. E. Knox, J. B. Cross, V. Bakken, C. Adamo, J. Jaramillo, R. Gomperts, R. E. Stratmann, O. Yazyev, A. J. Austin, R. Cammi, C. Pomelli, J. W. Ochterski, R. L. Martin, K. Morokuma, V. G. Zakrzewski, G. A. Voth, P. Salvador, J. J. Dannenberg, S. Dapprich, A. D. Daniels, O. Farkas, J. B. Foresman, J. V. Ortiz, J. Cioslowski and D. J. Fox, *Gaussian, Inc., Wallingford CT, 2009*.
- 55 E. Cancès, B. Mennucci and J. Tomasi, *J. Chem. Phys.*, 1997, **107**, 3032-3041.
- 56 Y. Noguchi and O. Sugino, *J. Chem. Phys.*, 2015, **142**, 064313.

Table 1 C–C and C–H bond lengths (in Å) of different rings in C₈₀H₃₀ and C₇₈H₃₀. R₅, R₆ and R₇ are averaged bond lengths of all five-, six-, and seven membered rings, R₆' is the averaged bond lengths of six-membered rings adjacent the five-membered ring.

	C ₈₀ H ₃₀				C ₇₈ H ₃₀
	R ₅	R ₆ '	R ₆	R ₇	R ₆
C–C	1.405	1.416	1.419	1.449	1.419
		1.418	1.426	1.450	1.426
		1.427	1.426	1.456	1.422
		1.421	1.423	1.456	1.399
		1.411	1.426	1.450	
			1.426		
Average	1.405	1.419	1.420	1.452	1.416
Exp. ^{33, 35}	1.409	1.421	1.422	1.455	
C–H			1.082		1.080

Table 2 HOMO, LUMO energies (in eV) and their gaps (in eV).

	HOMO	LUMO	Gap
Model I			
C6	-6.971	-0.319	6.651
C5-C6-C5	-5.433	-2.420	3.013
C5-C6-C7	-5.134	-2.455	2.680
C6-C6-C6	-5.962	-1.360	4.603
C7-C6-C7	-5.076	-2.528	2.548
Model II			
C5-C7	-5.068	-2.595	2.472
C5-C6-C7	-5.134	-2.455	2.680
C5-C6-C6-C7	-5.132	-2.438	2.695
C5-C6-C6-C6-C7	-5.189	-2.278	2.911
Model III			
C5C6	-6.039	-1.895	4.145
C5C6C6	-5.680	-1.846	3.835
C5C6C7	-5.260	-2.261	3.000
C5C6C6C7	-5.403	-2.087	3.317
Model IV			
180 °	-5.260	-2.261	3.000
175 °	-5.259	-2.263	2.996
170 °	-5.262	-2.269	2.993
165 °	-5.266	-2.279	2.987
160 °	-5.303	-2.282	3.021

Figure Captions

Fig. 1 Structures, optical absorption spectra (upper) of $C_{80}H_{30}$ and $C_{78}H_{30}$ molecules and their HOMO and LUMO orbitals (lower).

Fig. 2 B3LYP predicted structures and absorption spectra of $C_{78}H_{28}$ (**a**), $C_{76}H_{26}$ (**b1** and **b2**), $C_{74}H_{24}$ (**c1** and **c2**), $C_{72}H_{22}$ (**d**), and $C_{70}H_{20}$ (**e**). The structures were constructed by removing C and H atoms from $C_{80}H_{30}$.

Fig. 3 B3LYP predicted structures and absorption spectra of $C_{80}H_{32}$ (**a'**), $C_{80}H_{34}$ (**b1'** and **b2'**), $C_{80}H_{36}$ (**c'**), $C_{80}H_{38}$ (**d'**) and $C_{80}H_{40}$ (**e'**). The structures were constructed by adding H atoms to $C_{80}H_{30}$.

Fig. 4 Model molecules with various connections of C5, C6 and C7 rings

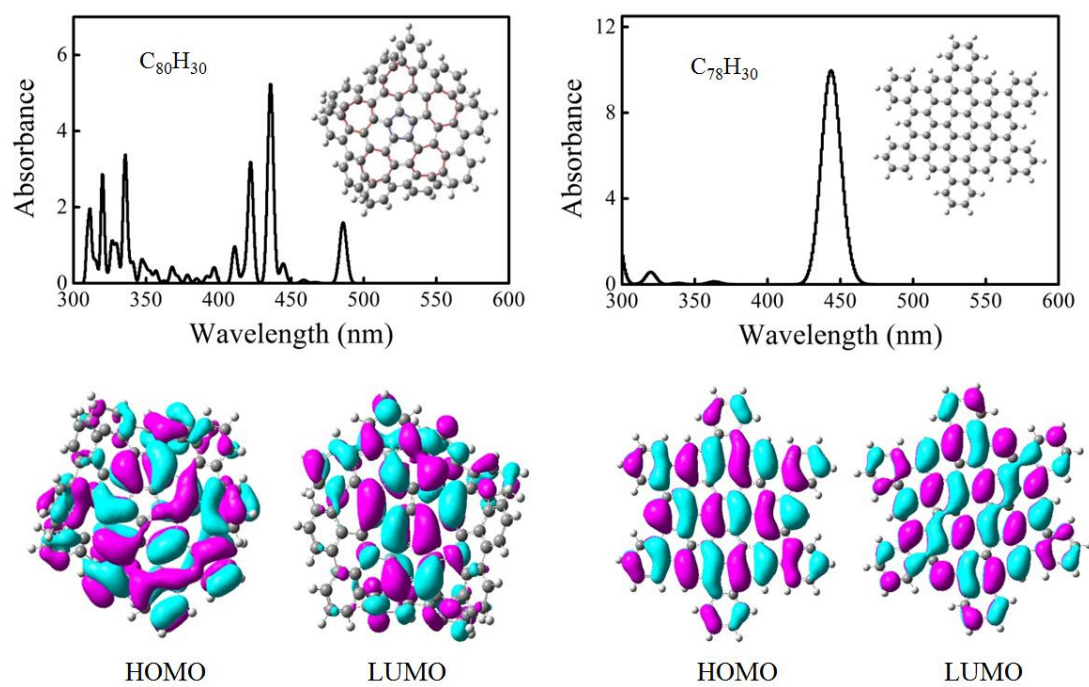


Fig. 1 Structures, optical absorption spectra (upper) of $C_{80}H_{30}$ and $C_{78}H_{30}$ molecules and their HOMO and LUMO orbitals (lower).

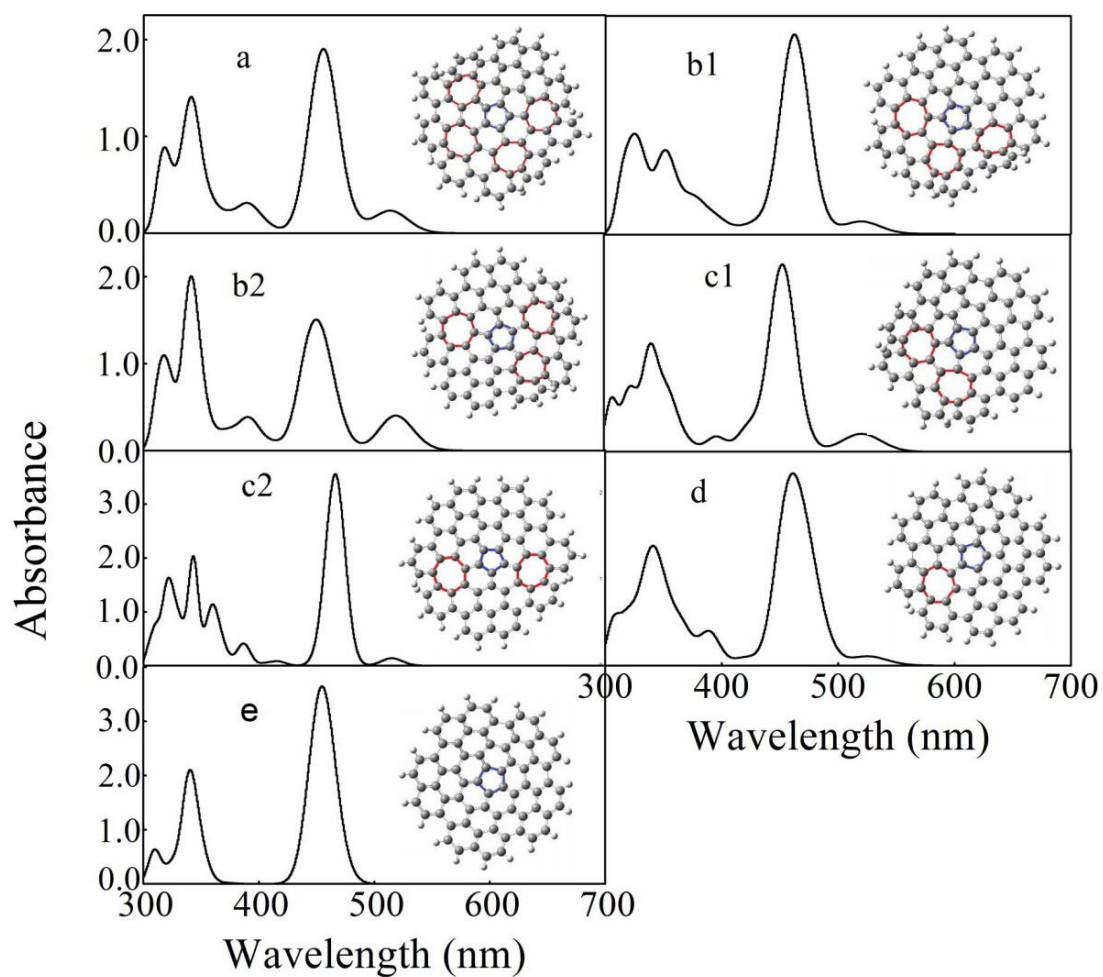


Fig. 2 B3LYP predicted structures and absorption spectra of $C_{78}H_{28}$ (**a**), $C_{76}H_{26}$ (**b1** and **b2**), $C_{74}H_{24}$ (**c1** and **c2**), $C_{72}H_{22}$ (**d**), and $C_{70}H_{20}$ (**e**). The structures were constructed by removing C and H atoms from $C_{80}H_{30}$.

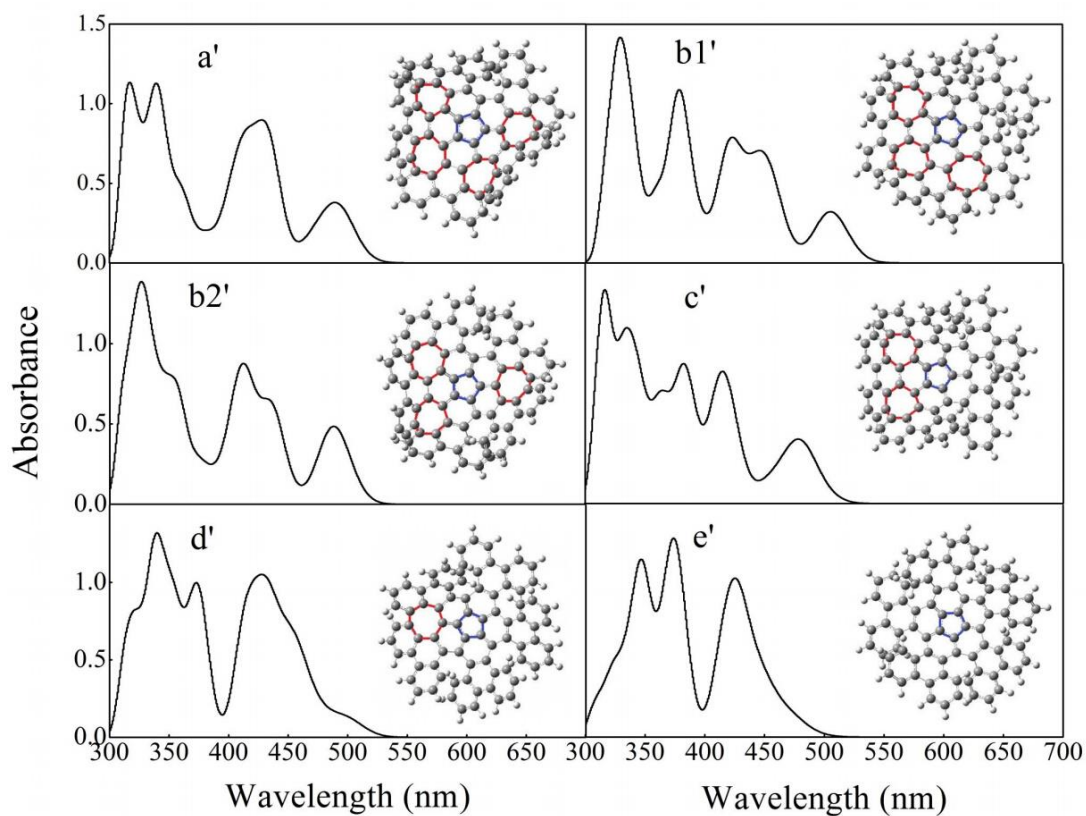


Fig. 3 B3LYP predicted structures and absorption spectra of $C_{80}H_{32}$ (**a'**), $C_{80}H_{34}$ (**b1'** and **b2'**), $C_{80}H_{36}$ (**c'**), $C_{80}H_{38}$ (**d'**) and $C_{80}H_{40}$ (**e'**). The structures were constructed by adding H atoms to $C_{80}H_{30}$.

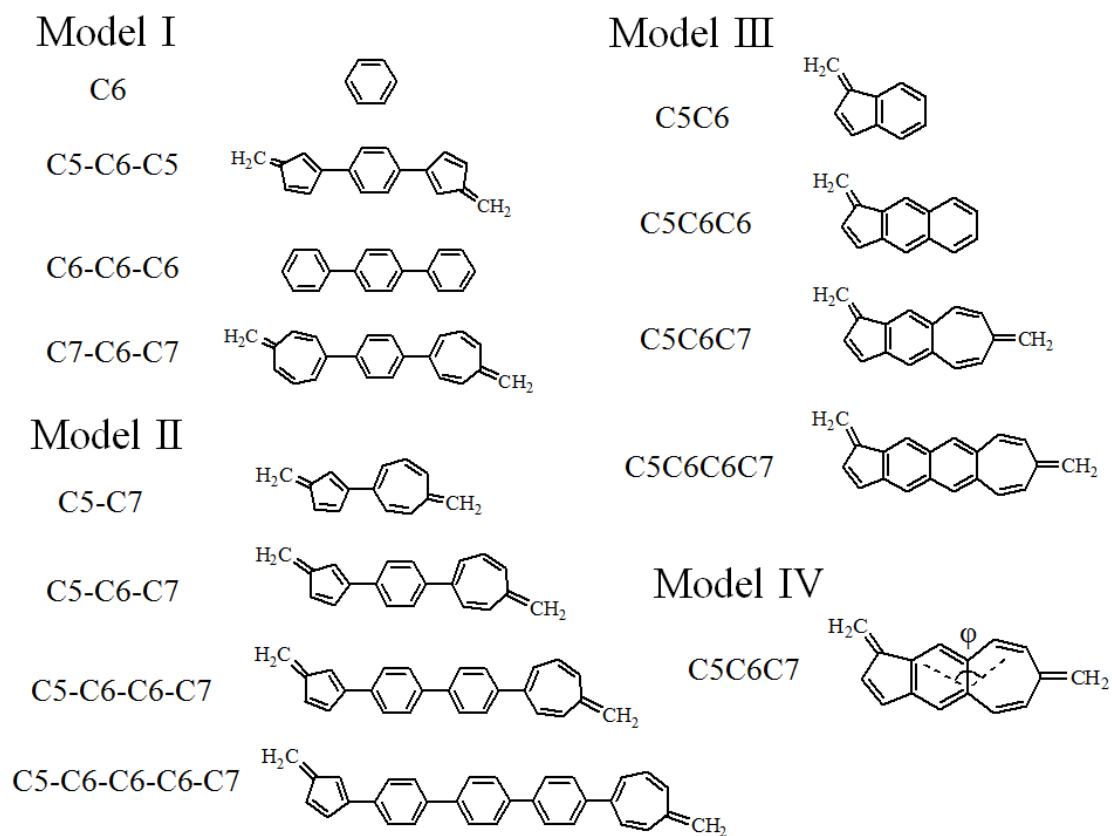


Fig. 4 Model molecules with various connections of C5, C6 and C7 rings